Quantitative Feedback Control of a Pendulum with Uncertain Payload

Withit Chatlatanagulchai[1]
Bundit Inseemeesak[2]
Control of Robot and Vibration Laboratory (CRV Lab),
Department of Mechanical Engineering, Faculty of Engineering,
Kasetsart University, Bangkok 10900, Thailand
(E-mail : [1]fengwtc@ku.ac.th, [2]Bundit288@hotmail.com)
Wichai Siwakosit
Department of Mechanical Engineering, Faculty of Engineering,
Kasetsart University, Bangkok 10900, Thailand
(E-mail : wichai.s@ku.ac.th)

Abstract

A controller design based on the quantitative feedback theory (QFT) is presented. QFT explicitly considers plant uncertainties during design phase. Frequency-domain specifications such as closed-loop stability margin, tracking, control effort, and disturbance and noise rejections are quantified as bounds for which the controller is loop-shaped. As a result, the controller is robust against uncertainties and disturbances, and the desired performance level can be specified quantitatively. We apply the controller to a pendulum having uncertain payload mass. Even in the presence of uncertainties, the controller performs very well as can be seen from both simulation and experimental results.

Key words: Quantitative Feedback Theory, Robust Control, Feedback Control, Plant Uncertainties, Pendulum, Uncertain Payload

1. Introduction

Feedback is required only for controlling systems with uncertainties. Despite this fact, most feedback control techniques are designed from fixed plant and hence cannot effectively handle uncertainties. Since system identification is not perfect, actual plant always deviates from the fixed plant. We need a design technique that explicitly and quantitatively takes uncertainties into account during the control design process.

Quantitative feedback theory (QFT) was devised almost fifty years ago by I. Horowitz [1]. It is a frequency-based design technique that extends the work of H.W. Bode [2] to a more quantitative way. The design is performed mainly on the Nichols chart, which is an integration of Bode's magnitude and phase plots. At a specific frequency, instead of being viewed as a point on the Nichols chart, the plant is now viewed as a template, which is an area containing possible plant values amidst uncertainties. This plant template is used throughout the design process, ensuring the design robustness.

Suppose we know the plant transfer function and its variations a priori; the plant templates can be generated on the Nichols chart. There are still three main tasks in QFT. First, we must obtain closed-loop specifications in frequency domain. Second, with the aid of the plant templates, frequency-domain specifications are used to calculate various bounds. A bound, belonging to a specific frequency, gives a valid region that the open-loop transfer function must lay. Third is the loop shaping process, where the controller is designed to shape the open-loop transfer function to be in the valid region.

Although QFT was originated decades ago, its applications have just been accelerated in the late 80s and early 90s due to the advent of the QFT computer-aided-design (CAD) packages [3]-[5]. Its applications range from control of continuous stirred tank reactor [6], idle speed control of automotive fuel injected engine [7], F-16 flight control system [8], waste water treatment control system [9], large wind turbine control systems [10], positioning a pneumatic actuator [11] to coordinated control of formation flying spacecraft [12].

QFT is claimed by the originator, I. Horowitz [13], to be applicable to wide variety of systems including the most difficult one, the nonlinear, time-

varying system. But in fact it is the use of the plant template that incorporates all plant uncertainties and makes the QFT one of the most versatile and practical control design techniques to date. Most people have regarded QFT as a trick of the trade, rarely seen in literature, and behind some of the most elegantly solved control problems that were deemed impossible. Unsurprisingly, over the course of five decades, the authors have found only four textbooks ([13]-[16]) in this subject, written by a small community of authors.

In this paper, we start with presenting some QFT basics with an attempt to organize some basic materials mostly scattered in the literature and to ease unfamiliar readers. We then present the quantitative feedback control design of a pendulum with uncertain payload. The payload has loose masses (Thai coins) inside; the jiggle makes the payload uncertain. Moving in the vertical plane, the pendulum has a nonlinear term, which makes the control problem more interesting.

The paper is organized as follows. Section 2 contains some QFT basics necessary to understand the content of this paper. Equation of motion, system identification, as well as plant templates of the pendulum are given in Section 3. Section 4 discusses controller design in three steps: obtaining the frequency-domain specifications, creating various bounds, and loop shaping. Simulation results are also given in Section 4. Section 5 contains experimental set-up and experimental results, and conclusions are given in Section 6.

2. QFT Basics

QFT can be applied to feedback systems depicted in Figure 1. Plant P represents a linear plant in a set $\{P\}$ that contains all possible variations due to uncertainties. The plant can have single or multiple inputs and outputs. H represents sensor transfer function. Controller G and prefilter F are to be synthesized to meet robust stability and closed-loop specifications. d_I and d_O are disturbances at plant input and output, together with their transfer functions P_{dI} and P_{dO}. $n, r, e, u,$ and y are sensor noise, reference input, error, control input, and plant output respectively.

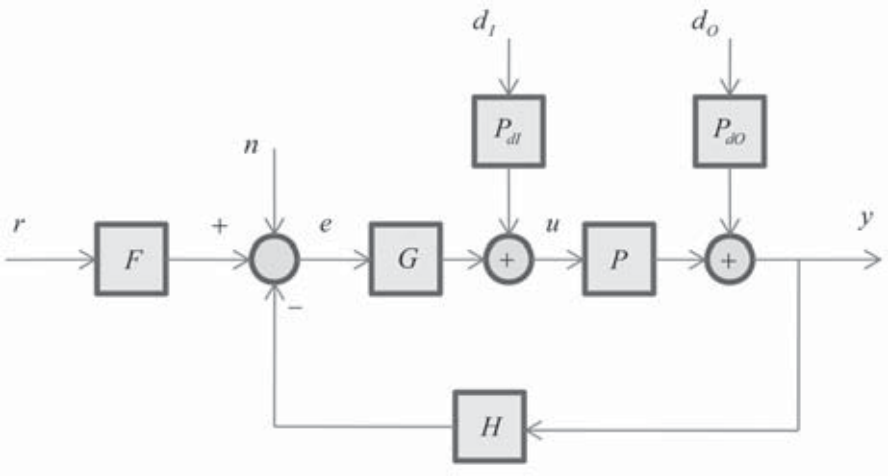

Figure 1 : Applicable feedback system.

Time-domain specifications are imposed on the plant output y and the plant input u. For stabilization, disturbance rejection, and disturbance attenuation problems, the plant output should be kept close to zero for given non-zero initial conditions or given disturbances. For tracking and regulation problems, the plant output should be bounded between upper and lower time functions, which are close to the reference input. The control effort for a given sensor noise, disturbances, or reference input is bounded by two given time functions often to avoid saturation.

Frequency-domain specifications are described in terms of inequalities on the system's transfer functions from some inputs to some outputs. Typically, they are as follows:

1) plant output disturbance rejection,

$$\left|y / d_O\right| = \left|P_{dO} / \left(1 + PGH\right)\right| < \delta_{dO}, \tag{1}$$

2) plant input disturbance rejection,

$$\left|y / d_I\right| = \left|P_{dI} P / \left(1 + PGH\right)\right| < \delta_{dI}, \tag{2}$$

3) model matching,

$$\left|y / r - F_m\right| = \left|PGF / \left(1 + PGH\right) - F_m\right| < \delta_m, \tag{3}$$

4) tracking,

$$\alpha \le \left| PGF/\left(1+PGH\right)\right| \le \beta, \tag{4}$$

5) noise rejection,

$$\left| y/n \right| = \left| PG/\left(1+PGH\right)\right| < \delta_n, \tag{5}$$

6) control effort,

$$\left| u/n \right| = \left| G/\left(1+PGH\right)\right| < \delta_c, \tag{6}$$

where all $\delta's$ are small positive numbers and α and β are numbers a little less than one and a little more than one respectively. $\delta's, \alpha$, and β can also be transfer functions with appropriate magnitudes. QFT problems are usually classified into one degree of freedom (DOF), where only the controller G is designed, and two degrees of freedom, where the controller G and the prefilter F are designed. Obviously, model matching and tracking problems are two DOFs, and the rest are one DOF.

Since QFT is designed in the frequency domain, whereas a true evaluation of a feedback system's performance is done in the time domain, translation of specifications from time domain to frequency domain is then necessary. There is no one-to-one translation, however; this constitutes a major loophole in QFT. Nevertheless, in practice, there exist some very good translation techniques. They are as follows. First, the closed-loop system can be approximated by a second-order transfer function whose roots directly reflects time-domain behavior (see chapter 3 of [13].) Second, the controller structure can be assumed a priori with unknown design parameters. Then possible range of each unknown design parameter can be found before the actual design process (see chapter 3 of [14].) Third, time-domain functions that represent specifications can be approximated followed by Laplace transformations to obtain frequency-domain transfer functions [17]. Fourth, the time-domain input-output pairs can be used in system identification to find transfer functions of desired time-domain specifications.

After frequency-domain specifications are obtained, the bounds can be calculated. The purpose of bound calculation is for designing of the controller G. There is one bound for one frequency ω and for one frequency-domain specification. Typically, we can obtain bounds in three ways [14]. First, using complex plane, for a frequency ω, a valid solution $G\left(j\omega\right)$ must lie outside of

a circle (for specifications (1)-(4)) or lie inside of a circle (for specifications (5)-(6).) For all plants $P \in \{P\}$, the union of all the circles can be calculated to form a bound $B(\omega)$, and $G(j\omega)$ can be designed to lie outside (or inside) of $B(\omega)$. Second, write $G(j\omega)$ and $P(j\omega)$ in polar forms $ge^{j\phi}$ and $pe^{j\theta}$ respectively. Each specification then produces an inequality in quadratic form whose g and ϕ can be computed by appropriate algorithms. Third, using Nichols chart, for a frequency ω and a fixed $G(j\omega)$'s phase ϕ, a nominal point on the plant template marks a point on a bound. The whole bound can be obtained by varying ϕ.

Loop shaping is the skill to generate a controller G such that an open-loop transfer function satisfies certain bounds. There is no fixed law on how to do so. It is totally up to the experience of the designers; hence, loop shaping is the most difficult stage for the novices. Some basic transfer functions are normally appended to the controller. They are:

1) Simple gain: k,

2) Integrator or differentiator:

$$\frac{1}{s^n} \text{ or } s^n,$$

3) Lead or lag:

$$\frac{s/z+1}{s/p+1},$$

4) Real pole or real zero:

$$\frac{1}{s/p+1} \text{ or } s/z+1,$$

5) Complex pole or complex zero:

$$\frac{1}{s^2/\omega_n^2+2\zeta s/\omega_n+1} \text{ or } s^2/\omega_n^2+2\zeta s/\omega_n+1,$$

6) Notch:

$$\frac{s^2/\omega_n^2+2\zeta_1 s/\omega_n+1}{s^2/\omega_n^2+2\zeta_2 s/\omega_n+1},$$

7) Complex lead:

$$\frac{s^2+2ads+a^2}{s^2+2bds+b^2}\frac{b^2}{a^2},$$

8) Super 2nd (2/2)

$$\frac{a_1s^2+a_2s+1}{b_1s^2+b_2s+1}.$$

Appending each basic transfer function to the open-loop transfer function $L(s)$ affects its gain and phase. The readers are advised to consult [15] for more details.

Design of the prefilter F is rather trivial. It can be shown (Chapter 3 of [14]) that, on a Bode magnitude plot, designing G to satisfy tracking bounds results in

$$\max_{P\in\{P\}}\log\left|\frac{PG(j\omega)}{1+L(j\omega)}\right|-\min_{P\in\{P\}}\log\left|\frac{PG(j\omega)}{1+L(j\omega)}\right|\le\log\frac{\beta(\omega)}{\alpha(\omega)}.$$

In words, G reduces the variation of the closed-loop transfer function's magnitudes to be narrower than the specifications. The task of F is to shift the closed-loop Bode plots so that they are within the specification boundaries.

3. A Pendulum with Uncertain Payload

We are interested in designing a QFT controller for a pendulum in the vertical plane whose free-body diagram is given in Figure 2. Using Newton's 2nd law, we have

$$T-(m_lga+m_bgb)\sin\theta=(I_l+I_b+m_la^2+m_bb^2)\ddot{\theta}. \tag{7}$$

The torque T is generated by a DC motor with the following equations

$$k_dV=IR_m+k_bk_g\dot{\theta}_2,$$
$$T=k_gk_mI,$$

where V is input voltage to motor driver, I is coil current, R_m is coil resistance, k_b is motor back-emf constant, k_b is gear ratio, k_d is motor driver constant, and k_m is motor torque constant. Combining the two equations above, we obtain

$$T = \frac{k_g k_m k_d V}{R_m} - \frac{k_b k_m k_g^2}{R_m}\dot{\theta}. \tag{8}$$

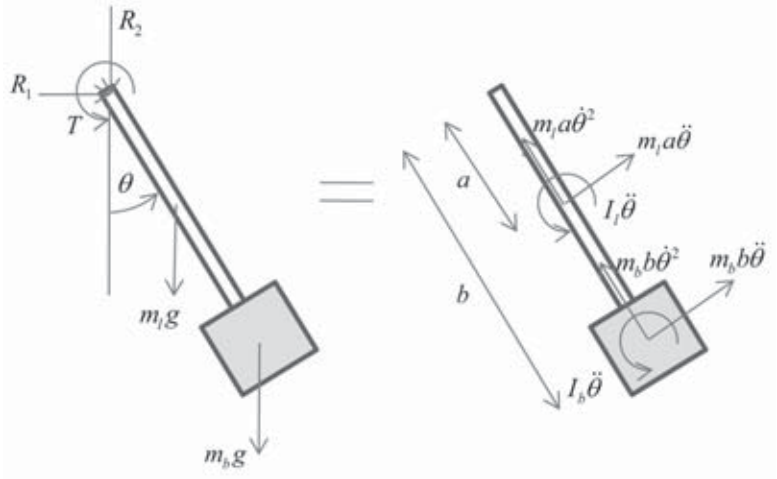

Figure 2 : Free-body diagram of a pendulum in vertical plane.

Substituting (8) into (7), letting $A = \left(I_l + I_b + m_l a^2 + m_b b^2\right)$, $B = \left(m_l g a + m_b g b\right)$, $C = k_g k_m k_d / R_m$, and $D = k_b k_m k_g^2 / R_m$, and rearranging terms, we obtain

$$V = \left[\ddot{\theta}, \dot{\theta}, \sin\theta\right]\begin{bmatrix} A/C \\ D/C \\ B/C \end{bmatrix}.$$

We can then set up the least-square algorithm as follows:

$$Y = \Phi\Theta,$$

where

$$\Phi \in \mathbb{R}^{n\times 3} = \begin{bmatrix} \ddot{\theta} & \dot{\theta} & \sin\theta \\ \vdots & \vdots & \vdots \end{bmatrix}, \Theta \in \mathbb{R}^{3\times 1} = \begin{bmatrix} A/C \\ D/C \\ B/C \end{bmatrix}, Y \in \mathbb{R}^{n\times 1} = \begin{bmatrix} V \\ \vdots \end{bmatrix},$$

n is the number of data points obtained from real experiment for system identification. To minimize the square error $E = \left(Y - \Phi\Theta\right)^2 / 2$, we have

$$\hat{\Theta} = \left(\Phi^T \Phi\right)^{-1} \Phi^T Y. \tag{9}$$

An actual hardware is set up, as detailed in Section 5, to obtain output data for determination of $\hat{\Theta}$. A frequency-varying sine signal, with frequencies from 0.1 Hz initially to 1 Hz at 100 seconds and amplitude of 0.5, is passed to the system as input V to the motor driver. The output θ is measured; its derivatives are obtained from finite differences. The vector of unknown variables $\hat{\Theta}$ can now be calculated using (9). Thirty-two experiments were performed to obtain ranges of unknown variables as follows:

$$0 < A/C < 0.0002,\ 0.15 < D/C < 0.35,\ 0.05 < B/C < 0.25. \tag{10}$$

Using an approximation $\sin\theta \approx \theta$ and applying the Laplace transformation to both sides of (7) and (8) lead to a plant transfer function from the motor driver's input to the angular position output as

$$\frac{\theta(s)}{V(s)} = \frac{1}{\frac{A}{C}s^2 + \frac{D}{C}s + \frac{B}{C}}. \tag{11}$$

Equation (11) represents pendulum's transfer function with parameter variations as given in (10). By letting $s = j\omega$, plant templates can be plotted on the Nichols chart as in Figure 3a for various frequencies. The asterisk marks position of the nominal plant, which is at $A/C = 0, D/C = 0.15,$ and $B/C = 0.05$.

4. Controller Design

We want the pendulum to track a square wave function. However, no system can ever track a square wave perfectly because no device can respond instantaneously to an input. There must be reasonable upper and lower bounds. To obtain bounds, we approximate the closed-loop system by a second-order transfer function

$$\frac{K\omega_n^2}{s^2 + 2\zeta\omega_n s + \omega_n^2}.$$

This is a well-known function whose ω_n is the natural frequency and ζ is the damping ratio. The gain K is used to adjust steady-state magnitude. For the lower bound, we let $\zeta = 1$ to obtain critically damped response and choose $\omega_n = 5$ for appropriate rise time. For the upper bound, we let $\zeta = 0.7$ to obtain

underdamped response and choose $\omega_n = 10$ for appropriate rise time, settling time, and maximum overshoot. The gain K for the lower and upper bounds are 0.95 and 1.05 respectively. The desired trajectory and tracking bounds are plotted in Figure 3b.

From Nyquist criterion, it can be shown that stability margin specification can be given in the form

$$\left|\frac{1}{1+L}\right| < \delta_s,$$

which is identical to the plant output disturbance rejection specification (1). We then choose $\delta_s = \delta_{dO} = 4dB$.

Later on, we will apply this controller to an actual system whose control effort is given to the system as input voltage to the motor driver, which must be within the range $(-2.5, 2.5)$. To avoid saturation, the control effort specification is then given by

$$|u/r| = |FG/(1+PG)| < \delta_c, \tag{12}$$

where $\delta_c = 2.5$.

So far, we have obtained three frequency-domain specifications: tracking (4), stability margin and plant output disturbance rejection (1), and control effort (12). Next step is to create frequency-domain bounds for the open-loop transfer function $L(s)$ on the Nichols chart. It can be shown [18] that $L(s)$ that satisfies the tracking and plant output disturbance rejection specifications must lie outside of an area enclosing the point $(-1,0)$ in the complex plane. On the Nichols chart, this valid region corresponds to the area above or outside of the bound. For control effort specification, it was shown in [14] that the valid region is inside of an area enclosing the origin in the complex plane, which is under or outside of the bound on the Nichols chart.

The tracking bounds are given in Figure 3c. We only imposed the tracking specifications on low frequencies (0.01 to 2 rad/s) to avoid unnecessarily high gain at high frequencies, which could amplify noise. Stability and plant output disturbance rejection bounds are shown in Figure 3d for whole range of frequencies. Due to the clutter, we can only highlight some low-frequency bounds. The bounds are closed because $|1/(1+L)| < 4dB$ produces a valid solution outside of an area that does not enclose the origin in the complex plane. The control effort bounds are given in Figure 3e. As

previously mentioned, a valid solution must lie under or outside of each bound for each frequency so that the control effort will be within the saturation limits. Figure 3f intersects all bounds and displays only the worst-case bounds.

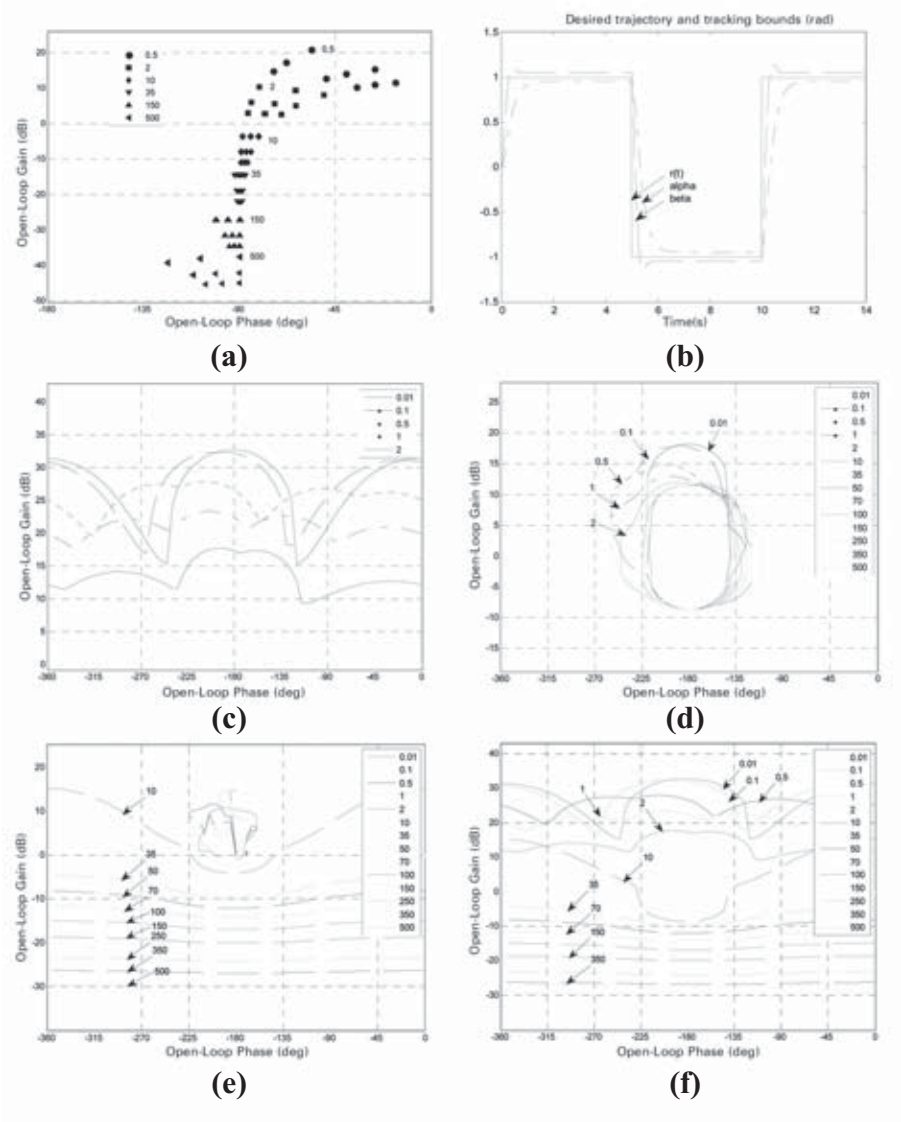

Figure 3 : (a) Plant templates on the Nichols chart at various frequencies.
(b) Desired trajectory and tracking bounds in time domain.
(c) Tracking bounds in frequency domain.
(d) Stability and plant output disturbance rejection bounds.
(e) Control effort bounds. (f) Worst-case bounds.

Once we obtain the intersection of all bounds. The controller $G(s)$ can be designed by shaping of $L(s)$ to satisfy all bounds on the Nichols chart. Figure 4a depicts initial $L(s)$ where $G=1$. After appending a gain, $L(s)$ is shifted upward as in Figure 4b so that the low-frequency bounds are satisfied; now $G(s)=2.178$. Looking closely, this seems to satisfy all bounds, and in fact we can stop here to obtain a famous proportional controller. However, there is a serious problem. The closed-loop system still has high bandwidth, which means not only high-frequency noise is amplified but also there are more chances that high-frequency modes are excited and cause instability. This is the reason we cannot increase the proportional gain forever. Figure 4c is the result after we append a real pole to decrease the high-frequency gains. We can see the lower gains at frequencies greater than 10 rad/s. At the current

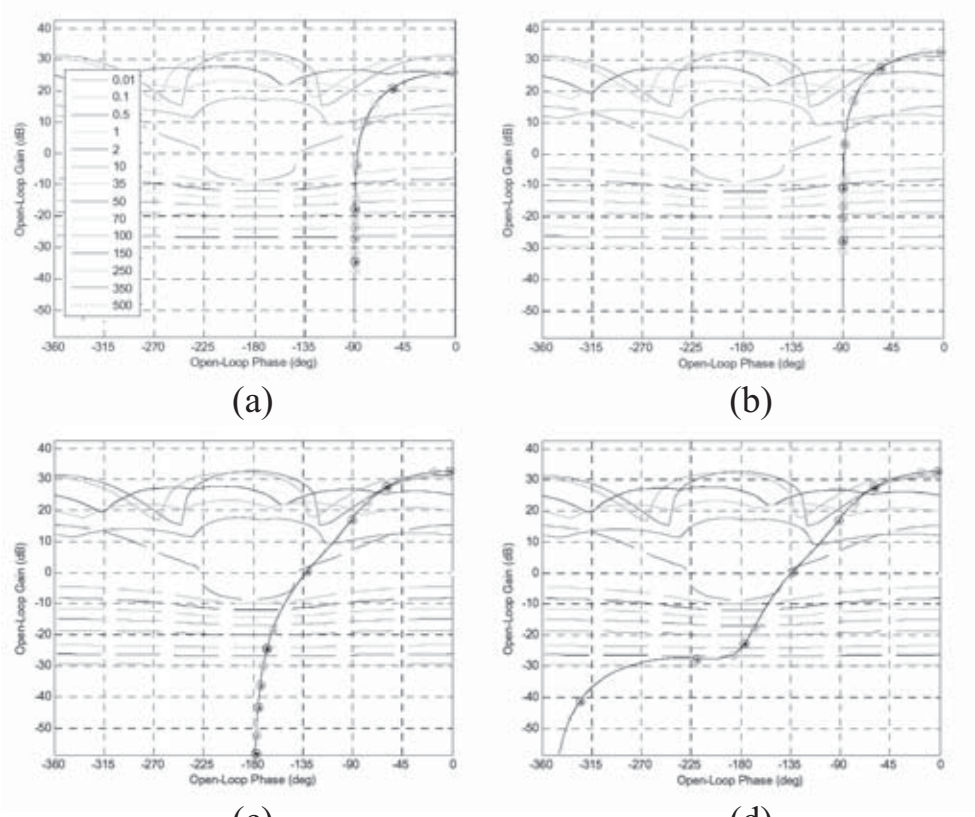

Figure 4 : (a) Initial open-loop. (b) After appending a gain.
(c) After appending a real pole.
(d) After appending a complex pole.

stage, $G(s) = 2.178/(s/10.65+1)$. Figure 4d shows the result of appending a complex pole to decrease gains further especially at high frequencies ($\omega > 150$ rad/s.) The final controller is given by

$$G(s) = \frac{2.178}{\left(\frac{s}{10.65}+1\right)\left(\frac{s^2}{115.5^2}+\frac{2(0.156)s}{115.5}+1\right)}. \tag{13}$$

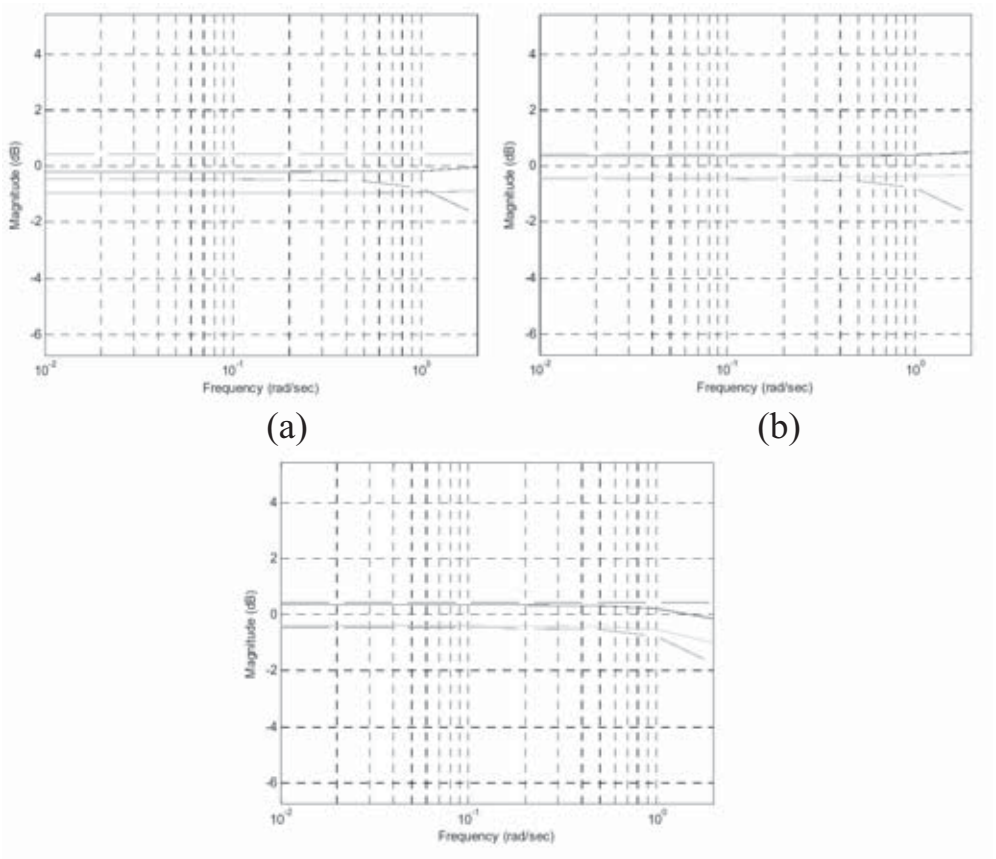

Figure 5 : (a) Initial closed-loop magnitudes with unit prefilter. Dashed lines are tracking bounds; solid lines are the closed-loop magnitudes.
(b) After appending a gain. (c) After appending a real zero.

The solid lines of Figure 5a show initial closed-loop magnitudes with $F(s) = 1$. The dotted lines are tracking specifications. We design the prefilter to shift the closed-loop magnitudes to be within the specifications. Figure 5b is

after a gain is appended, and Figure 5c is after a real zero is appended. The final prefilter is given by

$$F(s) = \frac{1.066}{\left(\frac{s}{4.935} + 1\right)}. \tag{14}$$

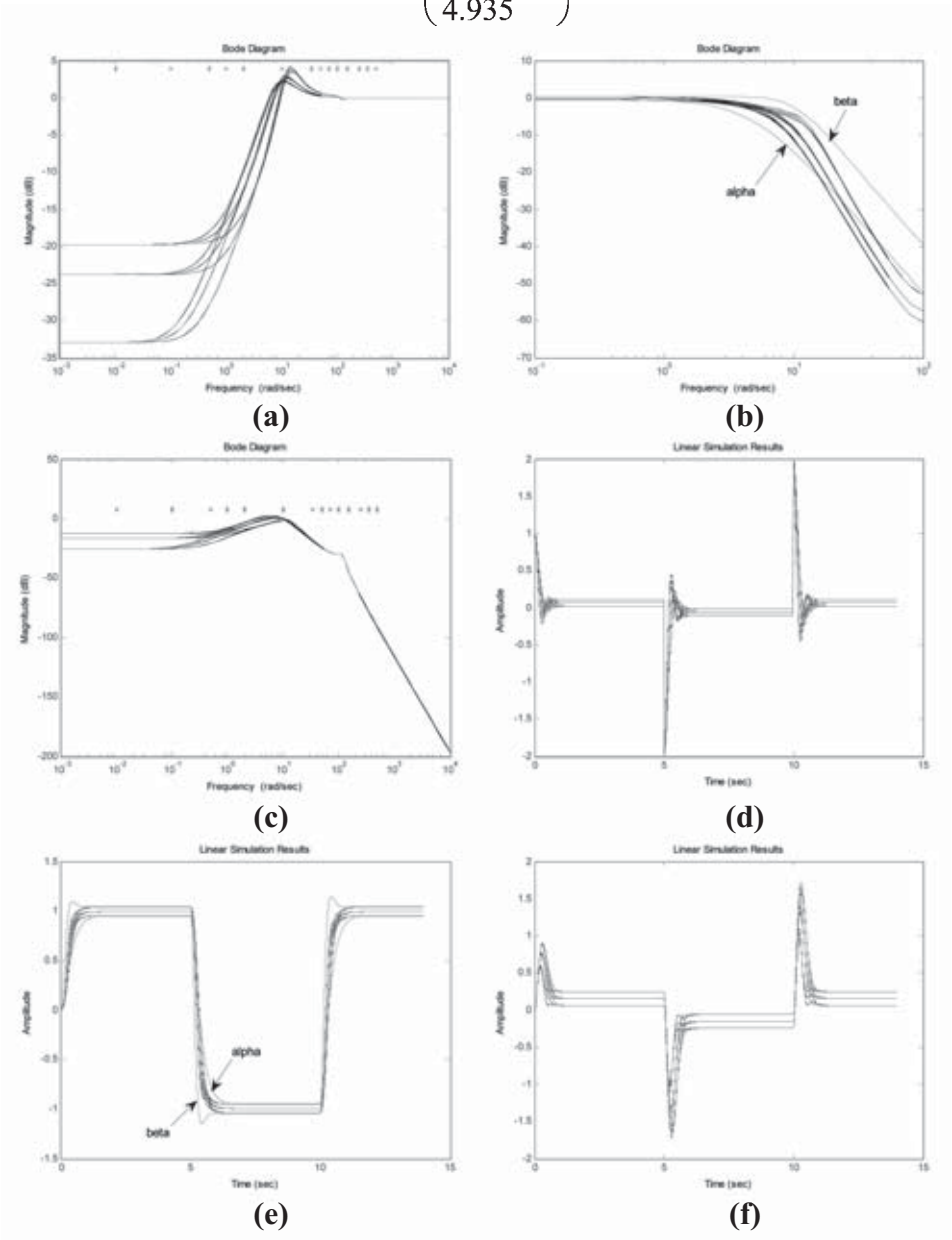

Figure 6 : Specifications and closed-loop performance in frequency domain: (a) stability, (b) tracking, (c) control effort. Time-domain system performances: (d) output disturbance rejection, (e) tracking, (f) control effort.

Simulation results are given in Figure 6. In Figure 6a, the asterisks represent stability and plant output disturbance rejection specifications of 4 dB at various frequencies. Solid lines are the magnitudes of the closed-loop transfer functions $1/(1+GP)$, where there are twenty-seven plant cases representing plant uncertainties. We can see that the magnitudes are well within the specifications except at frequencies around 15 rad/s, which have not been designed for. The performance can be improved easily by including this frequency in the design. The solid lines in Figure 6b are tracking specifications α and β respectively. For all plant cases, the closed-loop performance is well within the specifications upto about 10 rad/s. This is because we only included frequencies upto 2 rad/s in our design. Figure 6c shows that the control effort is lower than the specification of 2.5 volts for all frequencies.

In Figure 6d, a square wave identical to the reference input was given as the plant output disturbance. The solid lines are the system outputs obtained from the square-wave disturbance for all plant cases. We can see that the controller effectively attenuates the disturbance, ensuring the system robustness against plant output disturbances such as ground or table vibrations. Figure 6e shows the system tracking performance. The system outputs closely track the square-wave reference input and fall within specified bounds. We can also improve the tracking performance by tightening the tracking specifications further. Note that there is a tradeoff between tracking performance and control effort, however. At the beginning of each movement, that is, when $t \simeq 0, 5, 10, ...$ seconds, the system outputs are outside of the lower bound. This is well understood as mentioned in [13]; it is the result of estimating the closed-loop system with a second-order transfer function when the tracking specifications was devised. Figure 6f simulates the control efforts u from the square-wave reference input r for all plant cases. The control efforts are well within the (-2.5, 2.5) saturation limits.

5. Experimental Set-up and Results

Figure 7a depicts the actual pendulum used in our experiment. The payload mass is a chewing-gum box containing some Thai coins, which juggle when the pendulum moves. The link is made of thin aluminum sheet, which is quite flexible in the direction normal to the movement plane. There is an Omron optical encoder to measure angular position, a Faulhaber 12V DC motor to move the pendulum, and a Dimension Engineering motor driver to drive the motor.

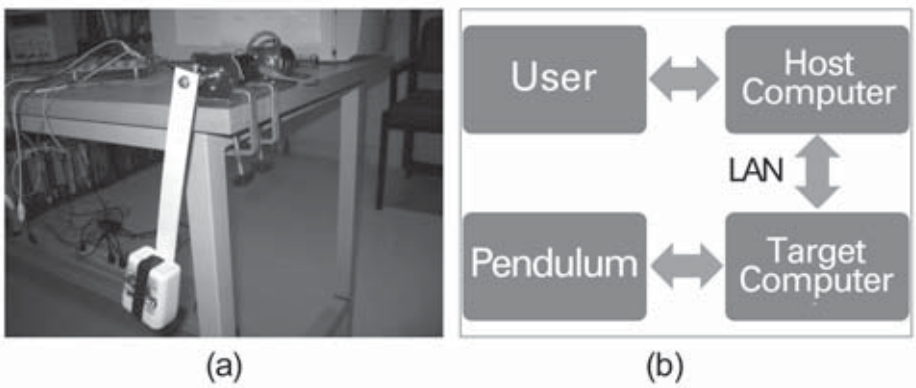

Figure 7 : (a) A pendulum with uncertain payload.
(b) Overall experimental set-up.

The overall experimental set-up is given in Figure 7b. User interfaces with the host computer via a monitor and a keyboard. The host computer runs Windows XP, Labview, Labview Real-Time, Labview Control Design Toolbox, Labview Simulation Module, and Matlab. The user develops real-time codes on the host computer before deploying to the target computer via a PC-to-PC LAN cable. The target computer is an embedded, stand-alone CPU running Labview Real-Time operating system and containing a DAQ card. The optical encoder sends channel-A and channel-B pulse trains to two digital input ports on the DAQ card to determine the angular position. An analog output channel sends control effort voltage to the motor driver to drive the motor. The saturation limits are (-2.5, 2.5) volts. A DC power supply supplies 12V current to the motor driver. The communication between the target and the host computers is bidirectional. The target computer acquires input-output signals and sends to the host computer to display to the user via the monitor. The user can send commands to the target computer via the keyboard.

We applied the controller (13) and the prefilter (14) to the actual pendulum. Sampling period of 0.001 seconds was used. Figure 8 shows the experimental results. From Figure 8b, the plant output is able to follow the reference input within its design upper and lower bounds. The control effort in Figure 8d is well within the saturation limits (-2.5, 2.5). The experimental result agrees with the simulation results in the previous section.

Next, the readers might be tempted to question whether the tracking result can be improved. We redesigned the controller and the prefilter by tightening the tracking specifications from

$$0.95\omega_n^2 / \left(s^2 + 2\zeta\omega_n s + \omega_n^2\right) \text{ and } 1.05\omega_n^2 / \left(s^2 + 2\zeta\omega_n s + \omega_n^2\right)$$

to

$$0.995\omega_n^2 / \left(s^2 + 2\zeta\omega_n s + \omega_n^2\right) \text{ and } 1.001\omega_n^2 / \left(s^2 + 2\zeta\omega_n s + \omega_n^2\right)$$

using the same ζ and ω_n as before. The new controller was redesigned to obey tracking and stability margin specifications but may violate the control effort specifications. The resulting controller and prefilter are

$$G(s) = \frac{7011.4814}{s + 199.8} \text{ and } F(s) = \frac{4.8542}{s + 4.844}.$$

Figure 9 shows experimental results. The actual output now falls within the new tracking specifications as seen from Figure 9b. From Figure 9d, we see that the saturation limits are in fact reached at some points. However, this is allowable because most motor drivers allow temporary peak of input current. Taking a closer look at the tracking error, we can see that, even with the presence of plant uncertainties, the controller is able to achieve the steady-state error of 0.00002 degrees or 20 micron.

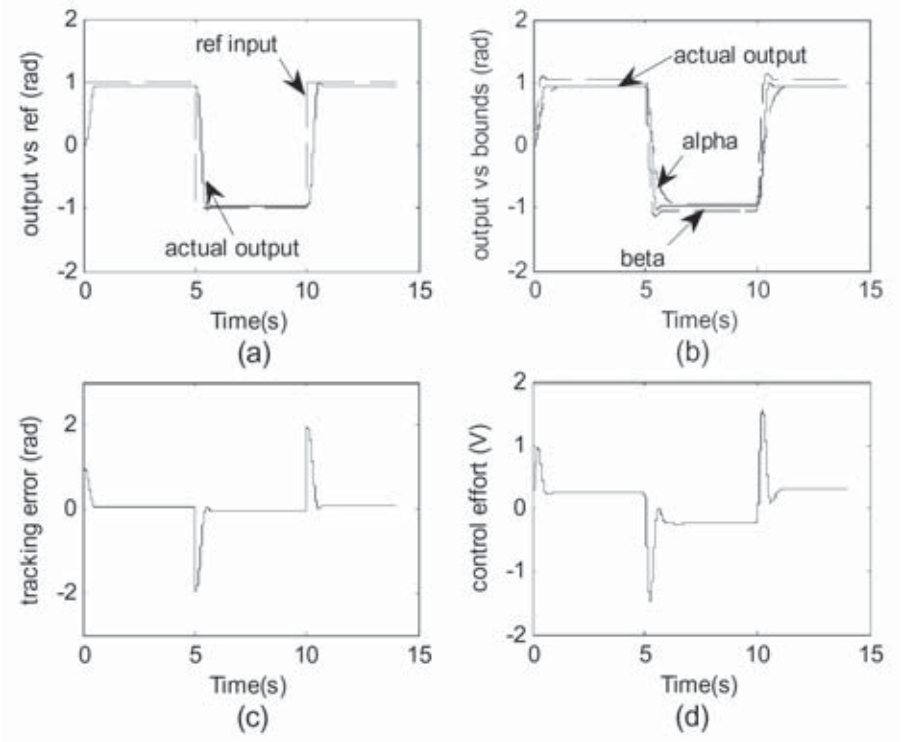

Figure 8 :(a) Plant output versus reference input.
(b) Plant output versus upper and lower bounds.
(c) Tracking error. (d) Control effort.

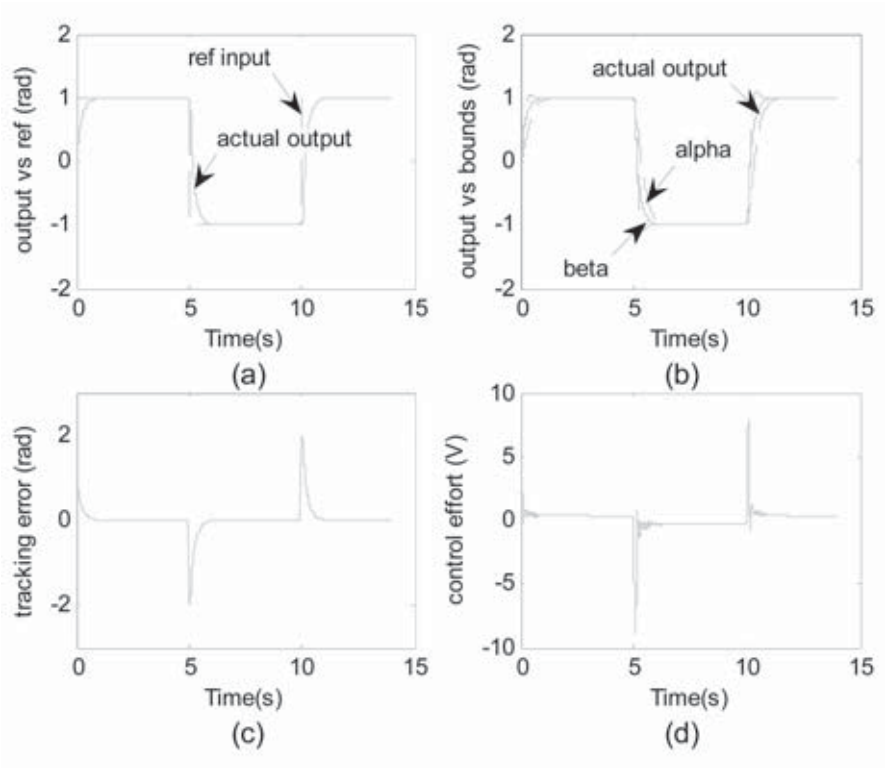

Figure 9 :(a) Plant output versus reference input.
(b) Plant output versus upper and lower bounds.
(c) Tracking error. (d) Control effort.

6. Conclusions

Both simulation and experimental results have shown the effectiveness of the QFT controller. Various specifications such as tracking accuracy, control effort saturation limits, stability margin, noise and disturbance rejections can directly be specified during the design process.

However, since QFT is a frequency-domain design technique, it requires linear plant. If actual plant varies a lot during operations, the size of the plant template will be too large in order to cover all plant cases, which will result in the QFT controller being overly conservative. Techniques, which permit on-line adaptation, such as adaptive control, neural and other intelligent controls, or even gain scheduling may be used to adjust plant parameters. But this may require an ability to loop-shape in real time.

Another area that requires more research is finding an effective way to translate time-domain to frequency-domain specifications. At this moment, there is no single technique suitable for any situations. There is a serious doubt that there will ever be such an effective technique.

QFT design of nonlinear system is an active research topic with slow progress. The present techniques are mostly based on linearization of the plant around operating points.

There are still rooms for improving the QFT designs for MIMO and cascaded systems since the present techniques mostly tend to be over-conservative or require design iteration.

7. Acknowledgement

The first author would like to thank Craig Borghesani and Terasoft, Inc for their evaluation copy of the QFT Matlab toolbox. This work is performed at the Control of Robot and Vibration Laboratory, which is situated at and partially supported by the Research and Development Institute of Production Technology (RDiPT) of Kasetsart University, Thailand.

8. References

[1] I. Horowitz, "Fundamental theory of linear feedback control systems," *Trans. IRE on Auto. Control*, AC-4, Dec. 5-19, 1959.

[2] H.W. Bode, *Network Analysis and Feedback Amplifier Design*, Van Nostrand, 1945.

[3] C. Borghesani, *Computer Aided-Design of Robust Control Systems Using the Quantitative Feedback Theory*, M.S. Thesis, Mechanical Engineering Department, University of Massachusetts, Amherst, MA, 1993.

[4] R.R. Sating, *Development of an Analog MIMO Quantitative Feedback Theory (QFT) CAD Package*, M.S. Thesis, Graduate School of Engineering, Air Force Institute of Technology, Wright Patterson AFB, OH, 1992.

[5] C.H. Houpis and G. Lamont, *Digital Control Systems: Theory, Hardware, Software*, McGraw-Hill, NY, 2nd Ed., 1992.

[6] C.H. Houpis and P.R. Chandler, Editors, *Quantitative Feedback Theory Symposium Proceedings*, Wright Laboratories, Wright-Patterson AFB, OH, 1992.

[7] M. Franchek and G.K. Hamilton, "Robust controller design and experimental verification of I.C. engine speed control," *Int. J. of Robust and Nonlinear Control,* vol. 7, pp. 609-628, 1997.

[8] S. Phillips, M. Pachter, and C.H. Houpis, "A QFT subsonic envelope flight control system design," *Proceedings of National Aerospace Electronics Conference,* Dayton, OH, May 1995.

[9] M. Garcia-Sanz and J.X. Ostolaza, "QFT-control of a biological reactor for simultaneous Ammonia and Nitrates removal," *International Journal on Systems, Analysis, Modeling, Simulation,* No. 36, pp. 353-370, 2000.

[10] E. Torres and M. Garcia-Sanz, "Experimental results of the variable speed, direct drive multipole synchronous wind turbine: TWT1650," *Wind Energy,* vol. 7, no. 2, pp. 109-118, 2004.

[11] M. Karpenko and No. Sepehri, "QFT design of a PI controller with dynamic pressure feedback for positioning a pneumatic actuator," *Proc. of the American Control Conference,* Boston, MA, pp. 5084-5089, June 2004.

[12] M. Garcia-Sanz and F.Y. Hadaegh, "Coordinated load sharing QFT control of formation flying spacecrafts. 3D deep space and low earth keplerian orbit problems with model uncertainty," *NASA-JPL, Jet Propulsion Laboratory Document,* D-30052, August 2004, Pasadena, California, USA.

[13] I. Horowitz, *Quantitative Feedback Design Theory – QFT,* QFT Publications, CO, USA, 1993.

[14] O. Yaniv, *Quantitative Feedback Design of Linear and Nonlinear Control Systems,* Kluwer Academic Publishers, Boston, USA, 1999.

[15] C.H. Houpis, S.J. Rasmussen, and M. Garcia-Sanz, *Quantitative Feedback Theory: Fundamentals and Applications, 2nd Edition,* CRC, 2005.

[16] M. Sidi, *Design of Robust Control Systems from Classical to Modern Practical Approaches, 1st Edition,* Krieger Publishing, 2001.

[17] K.R. Krishnan and A. Cruickshanks, "Frequency domain design of feedback systems for specified insensitivity of time-domain response to parameter variations," *International Journal of Control,* vol. 25, no. 4, pp. 609-620, 1977.

[18] C. Borghesani, Y. Chait, and O. Yaniv, *The QFT Frequency Domain Control Design Toolbox User's Guide,* Terasoft Inc, 2003.